COMPARISON OF MODELING OF THE POLAR CAP ABSORPTION EFFECT WITH OBSERVATIONS AT THE AARI GROUND-BASED NETWORK

A.V. Dmitriev (ID)
Skobeltsyn Institute of Nuclear Physics,
Lomonosov Moscow State University,
Moscow, Russia, dalexav@mail.ru

S.A. Dolgacheva (ID)
Arctic and Antarctic Research Institute,
St. Petersburg, Russia,
dolgachyova2010@yandex.ru

O.A. Troshichev (ID)
Arctic and Antarctic Research Institute,
St. Petersburg, Russia,
olegtro@aari.ru

M.S. Pulinets
Skobeltsyn Institute of Nuclear Physics,
Lomonosov Moscow State University,
Moscow, Russia, cotopaxy@gmail.com

Abstract. An elliptical model of cutoff for solar cosmic rays (SCR) at high latitudes has been calculated for SCR events and geomagnetic storms that occurred in February, March, and September 2014, June 2015, and September 2017 in order to predict the polar cap absorption (PCA) effect. The prediction is compared with observations of the PCA effect at the AARI network of six ionosondes, located in the north of Russia in a wide range of longitudes from 30° to 170° and magnetic latitudes from 56° to 64°. We examine the dependence of the cutoff latitude on the magnetic storm strength, as well as the effect of additional ionization of the dayside and nightside ionosphere by SCR protons and electrons. The model demonstrates a satisfactory statistical accuracy up to 0.83 for the PCA prediction. We discuss prospects for further improvement of the elliptical model, such as consideration of the impact of SCRs of higher energies and inclusion of the *PC* index of energy flux into the polar cap.

Keywords: solar cosmic rays, geomagnetic cutoff, high-latitude ionosphere, ionosondes, polar cap absorption.

INTRODUCTION

Energetic protons and electrons of solar cosmic rays (SCRs) have energies from hundreds of keV to several GeV [Kallenrode, 2003], therefore they can penetrate into Earth's atmosphere in the polar caps at high latitudes; and high-energy SCRs, also at midlatitudes ($\gtrsim 50°$ geomagnetic latitude). Penetration of charged particles from the interplanetary medium into Earth's magnetosphere is bounded in latitude by rigidity of particles proportional to the energy. The lowest latitude at which a particle of certain rigidity can reach Earth's surface is defined as cutoff latitude for this rigidity [Kress et al., 2010].

Determination of cutoff latitude is the subject of numerous theoretical and experimental studies [Birch et al., 2005; Smart, Shea, 2009; Dmitriev et al., 2010]. The cutoff latitude has been shown to decrease with increasing rigidity. Due to the asymmetry of the geomagnetic field, the cutoff latitude for particles of this type depends on local time, as well as on the geomagnetic disturbance level: the cutoff latitude decreases during magnetic storms, especially at night and in the evening.

The interaction of SCRs with the upper atmosphere causes ionization to increase, which is directly observed in the electron content profiles at high latitudes [Dmitriev et al., 2008]. SCR protons and electrons produce additional ionization in the D and E layers of the ionosphere. In particular, SCRs with energies from several to tens of MeV cause increased ionization in the D layer at <90 km, which brings about the effect of cosmic radio noise absorption in the atmosphere. This effect is usually measured by riometers at 30–40 MHz [Little, Leinbach, 1958, 1959].

On the other hand, increased ionization in the E-region at heights of ~100 km of the so-called sporadic radiation E layer (E_{sr}) is caused by SCR electrons and protons with energies from hundreds of keV to several MeV. The E_{sr} effect is observed by ionosondes at 1–10 MHz. Intense SCR precipitation results in strong ionization of the upper atmosphere, which leads to scattering and complete absorption of radio waves — the so-called blackout effect [Rodger et al., 2006].

The SCR protons with energies of tens of MeV were originally believed to be responsible for the blackouts. Some studies, however, indicate that protons with an energy of several MeV and electrons with an energy of hundreds of keV contribute significantly to the blackout [Clilverd et al., 2007; Dmitriev et al., 2010]. Recent studies [Heino, Partamies, 2020] of the polar cap absorption (PCA) effect for cosmic radio noise have shown that the elliptical model of SCR cutoff for >2.5 MeV protons and >100 keV electrons demonstrates the highest accuracy in predicting SCRs [Dmitriev et al., 2010]. PCA effects were determined at meridional chains of riometers, located in Canada and northern Europe, for 73 SCR events with >10 MeV proton fluxes above 10 $(cm^2\ s\ sr)^{-1}$ in 1997–2010.

In this paper, we employ an elliptical cutoff model [Dmitriev et al., 2010] to predict the effects of absorp-

tion and formation of the E$_{sr}$ layer from data obtained by AARI vertical sounding ionosondes, located in the Russian Arctic sector. We examine four intervals of SCR enhancements with intense fluxes of >2.5 MeV proton and/or >100 keV electrons in solar cycle 24 from 2010 to 2020. The model is described in Section 1. Section 2 presents experimental data on SCRs and PCA. Comparison between the PCA model calculation and observations is made in Section 3 and is discussed in Section 4.

1. ELLIPTICAL MODEL

The elliptical model of cutoff for SCRs in the polar caps is detailed in [Dmitriev et al., 2010]. The model allows us to calculate the geomagnetic cutoff latitude λ for SCR protons and electrons with respective energies from 0.24 to >140 MeV and >300 keV in the Northern and Southern hemispheres depending on rigidity of SCR particles R, local time MLT, geodipole tilt angle PS, and the hourly geomagnetic indices Dst, K_p, and AE. Below is a brief description of the model for the Northern Hemisphere.

The cutoff boundary of particles of this type and rigidity is represented as an ellipse in an invariant coordinate system centered at the geomagnetic poles (see Figure 1). This coordinate system uses the local geomagnetic time rMLT: rMLT=6+MLT. Parameters of the ellipse, major as and minor bs semi–axes, the position of its center (X_0, Y_0), and the tilt angle φ about the dawn–dusk terminator are a function of the model parameters. Knowing parameters of the ellipse, for any given rMLT we can find the colatitude Λ and the geomagnetic cutoff latitude λ=90°–Λ.

For SCR protons under undisturbed geomagnetic conditions, the semi-axes of the ellipse as_q and bs_q as function of R are determined by the following expressions:
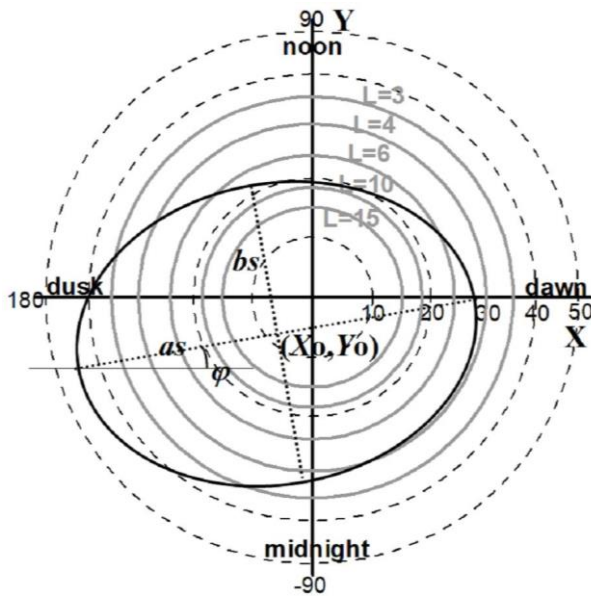

Figure 1. Coordinate system {rMLT, Λ} and elliptical approximation parameters: Λ is the invariant colatitude; rMLT is the geomagnetic local time (in degrees), counted from the dawn meridian (X-axis). Gray circles mark different L shells. The ellipse is indicated by as, bs, (X_0, Y_0), φ

$$\sin^4\left(as_q\right) = 2.41\cdot10^{-2} + 6.23\cdot10^{-5}R - -1.26\cdot10^{-2}\exp\left(-2.19\cdot10^{-2}R\right), \tag{1a}$$

$$\sin^4\left(bs_q\right) = 2.11\cdot10^{-2} + 6.21\cdot10^{-5}R - -1.19\cdot10^{-2}\exp\left(-1.81\cdot10^{-2}R\right). \tag{1b}$$

Under disturbed conditions, the complex dynamics of cutoff boundaries with a change in control parameters is modeled using multiparametric linear regression. Due to strong nonlinearity, changes in the semi-axes Δas and Δbs are modeled:

$$\Delta as = as - as_q, \tag{2a}$$

$$\Delta bs = bs - bs_q. \tag{2b}$$

The regression coefficients are linear functions of logarithmic proton rigidity, hence the general expression for Δas, Δbs, X_0, Y_0, and φ is written as follows:

$$P = A_0 + B_0 \log R + \left(A_{Dst} + B_{Dst}\log R\right)Dst + +\left(A_{K_p} + B_{K_p}\log R\right)K_p + \left(A_{PS} + B_{PS}\log R\right)PS. \tag{3}$$

The approximation coefficients A_i and B_i are listed in Table 1.

As a result, for this rMLT we can calculate the geomagnetic cutoff latitude of SCR protons as a point on the elliptical boundary, which is determined by R, Dst, K_p, and PS:

$$\lambda = 90° - \sqrt{x^2 + y^2}, \tag{4a}$$

$$x = X_0 + as\cos r\,\text{VLT}\cos\varphi - bs\sin r\,\text{MLT}\sin\varphi, \tag{4b}$$

$$y = Y_0 + as\cos r\,\text{MLT}\sin\varphi + bs\sin r\,\text{MLT}\cos\varphi. \tag{4c}$$

Here, as, bs, X_0, Y_0, and φ are found from Equations (1), (2), (3).

In the case of SCR electrons, the model is calculated in a similar way for as, bs, X_0, Y_0, φ as a linear regression for Dst, K_p, AE, PS:

$$P = P_0 + P_{Dst}\,Dst + P_{K_p}\,K_p + P_{PS}\,PS + P_{AE}\,AE.$$

The regression coefficients are given in Table 2.

The elliptical model was used to predict the PCA effect for three stations of the Canadian Advanced Digital Ionosondes (CADI) [Jayachandran et al., 2009] during a long period of SCR enhancements from December 6 to December 16, 2006 [Dmitriev et al., 2010]. The CADI stations are located near the 270° meridian in the latitude range 62.8°–80° N. The absence of reflection of a radio signal with a frequency of 4 MHz from the F layer at >100 km was a sign of PCA, which was associated with higher ionization of the D and E layers driven by intense SCR energetic particle fluxes.

Hour intervals were modeled; in each interval for particles of this type, the minimum cutoff latitude λ was calculated and their maximum flux F was determined. PCA was considered predicted by the model if the maximum particle flux F exceeded a certain threshold value F_{th} and the latitude λ was lower than the geomagnetic latitude

Table 1

Coefficients of elliptical approximation of cutoff boundaries for protons

North PCA	A_0	B_0	$A_{Dst}\cdot 10^{-2}$	$B_{Dst}\cdot 10^{-2}$	$A_{Kp}\cdot 10^{-2}$	$B_{Kp}\cdot 10^{-3}$	$A_{PS}\cdot 10^{-2}$	$B_{PS}\cdot 10^{-2}$
Δas	−.568	0.	−9.74	1.16	8.55	−7.46		
Δbs	−.648	0.	−9.54	1.16	7.66	−7.49		
X_0	−0.29	0.13	3.68	−544	−2.94	3.40		
Y_0	−9.26	1.53	−5.43	.827	−6.60	10.5	−7.40	1.12
φ	−54.9	11.3						

Table 2

Coefficients of elliptical approximation of cutoff boundaries for >300 keV electrons

North PCA	P_0	$P_{Dst}\cdot 10^{-2}$	$P_{Kp}\cdot 10^{-2}$	$P_{PS}\cdot 10^{-2}$	$P_{AE}\cdot 10^{-4}$
as	18.9	−4.3	9.86		
bs	17.1	−4.97	8.42		
X_0	0.758	.482	−2.58		
Y_0	−5.47			−4.68	4.67
φ	17.6	−67.		178.	

of the station λ_0, i.e. these particles caused sufficiently strong ionization over the station. The threshold value F_{th} is a free parameter of the model and is found by fitting model PCA to observations, as will be shown below.

When comparing model outputs with PCA observations at different stations, statistics (time in hours) on *HT*, *MT*, *FA*, *CR* were compiled, as shown in Table 3. For example, *HT* (Hit) accumulates intervals when PCA observations and predictions agree; *MT* (Miss) corresponds to the inability of the model to predict PCA; *FA* (False Alarm) stands for an erroneous model prediction of PCA, whereas it is not actually observed; *CR* (Correct Rejection) is the correct model prediction of PCA absence. Obviously, the sum of all statistics is equal to the total duration of the analyzed interval $N=HT+MT+FA+CR$.

Table 3

Statistical table for PCA

Model/Observation	With PCA	No PCA
$\lambda \leq \lambda_0$, $F \geq F_{th}$	HT	FA
$\lambda > \lambda_0$, $F < F_{th}$	MT	CR

From these statistics, statistical ratios were calculated: *PCP* (Probability of Correct Prediction) and *OUR* (Overestimation Underestimation Ratio):

$$PCP = (HT + CR)/N, \tag{5}$$

$$OUR = (HT - FA)/HT + FA. \tag{6}$$

The *PCP* parameter demonstrates how well the model is able to correctly predict PCA hour intervals: *PCP*=0 — complete inability, *PCP*=1 — perfect prediction of all intervals. The *OUR* parameter shows how balanced the model is. If the model systematically predicts false PCA, *OUR* approaches 1 or −1. For an ideal model, *OUR*=0.

By varying types of particles (cutoff latitudes λ) and their threshold fluxes F_{th}, we have obtained the best PCA

model for all three CADI stations with a maximum *PCP*=0.77 and *OUR*=0 for the following SCR particles: 2.5–6.9 MeV protons with F_{th}=100 $(cm^2 \ s \ sr)^{-1}$ and >100 keV electrons with F_{th}=2900 $(cm^2 \ s \ sr)^{-1}$.

In this study, for a detailed comparative analysis of the elliptical model and PCA effects, we use additional statistical parameters *POD* (Probability of Detection) and *FAR* (False Alarm Rate):

$$POD = HT/(HT + MT), \tag{7}$$

$$FAR = FA/(HT + FA). \tag{8}$$

The POD parameter shows how well the model is able to predict the PCA effect: *POD*=0 — complete inability; *POD*=1 — perfect prediction of all PCA intervals. The *FAR* parameter describes how often the model makes false predictions of PCA: *FAR*=0 — there are no false predictions; *FAR*=1 — all model predictions of PCA are false.

2.   DATA

The data on SCR electron and proton fluxes was obtained from measurements made at the ACE interplanetary monitor by the instrument EPAM with a time resolution of 5 min [Gold et al.,1998]. The data is available on [https://cdaweb.gsfc.nasa.gov/]. We examine four intervals of SCR enhancements in solar cycle 24 (2010–2020), in which >1.91 MeV proton fluxes exceeded the threshold intensity F_{th}=100 $(cm^2 \ s \ sr)^{-1}$ and/or >103 keV electron fluxes exceeded F_{th}=2900 $(cm^2 \ s \ sr)^{-1}$. The intervals are listed in Table 4. An important selection criterion was the presence of magnetic storms during the SCR enhancements.

The storm intensity is characterized by a minimum *Dst* variation, which is also shown in Table 4. Data on *Dst*, K_p, and *AE* is available in the World Data Center in Kyoto [https://wdc.kugi .kyoto-u.ac.jp/wdc/Sec3.html].

Experimental data on PCA was obtained from the AARI network of ionosondes of vertical sounding of the ionosphere (VSI), located in the Russian Arctic sector (Figure 2) [Kalishin et al., 2020]. The VSI stations employ

Table 4

Intervals of SCR enhancements

Beginning–end of SCR interval	Minimum *Dst*, nT
26.02–03.03.2014	–97
10.09–14.09.2014	–88
20.06–26.06.2015	–198
04.09–16.09.2017	–122

the Canadian Advanced Digital Ionosonde (CADI) that scans the ionosphere in the frequency range 1–13 MHz with a step of 0.024 MHz in the altitude range 90–1024 km with a step of 1 km [Vystavnoi et al., 2013]. Unfortunately, there were no observations for the selected intervals at the TIK station.

The VSI stations are listed in Table 5. Their refined geomagnetic coordinates *mLat* and *mLon*, calculated for the corresponding epochs, are also given there. The stations are clearly seen to have a very wide spread in latitude ~8° and a record wide spread in longitude ~110°. This promotes analysis of local time asymmetries of PCA, such as day–night and dawn–dusk.

The PCA effect was determined from VSI experimental data as the absence of reflection of radio signals in the frequency range 1–4 MHz from the ionosphere above 100 km. Figure 3 exemplifies the dynamics of ionospheric conditions during the February 2014 event. The top panel displays frequency parameters of the ionosphere: f_{min} — the minimum frequency observed in VSI ionograms; $f_o E_s$, $f_o F2$ — the critical frequencies of the ordinary wave of the E_s and F2 layers; $f b E_s$ — the

shielding frequency of the E_s layer; fxI — the highest frequency at which there are reflections from the F-region. The middle panel exhibits height parameters of the ionosphere: hE_s and $hF2$ are the minimum actual heights of the E_s and F2 layers. The bottom panel shows *Dst*.

The line "reflection type" in the top panel of Figure 3 indicates the presence of an echo up to 4 MHz in the ionograms. The 4 MHz frequency was chosen in order to preserve the conditions for determining PCA used in constructing the elliptical model of PCA [Dmitriev et al., 2010]. Mark 1 indicates the intervals when there is a reflection from the F-region of the ionosphere. Mark 2 means shielding of the F-region by the E_{sr} layer. Mark 0 stands for intervals when radio signals in the frequency range 1–4 MHz (or in the entire frequency range of the ionosonde) are absent at all heights. In this case, a signal could be scattered or reflected at <90 km, and also ionization might have been very weak with critical frequencies <1 MHz.

The PCA effect was identified as the presence of marks 0 or 2. In the last case, the E_{sr} layer is believed to be produced by ionization of the upper atmosphere by energetic SCR particles.

Using this method, hour intervals were determined for all the stations for the four selected intervals of SCR enhancements when at least one 15 min interval had a PCA effect. Figure 4 for six VSI stations shows hours with PCA (dark blue) and geomagnetic indices for the SCR events and magnetic storms in February–March and September 2014, June 2015 and September 2017.

Table 5

Coordinates of VSI stations of the AARI network

| Code	Observation station	Geographic latitude and longitude	*mLat, mLon* 2014	*mLat, mLon* 2015	*mLat, mLon* 2017.
GRK	Gorkovsraya	60.27° N, 29.38° E	56.83, 116.96	56.84, 116.95	56.89, 116.82
SAH	Salekhard	66.52° N, 66.67° E	58.39, 150.03	58.43, 150.04	58.53, 149.97
AMD	Amderma	69.60° N, 60.20° E	61.97, 146.76	62.01, 146.76	62.1, 146.67
LOZ	Lovozero	68.00° N, 35.02° E	63.34, 126.8	63.37, 126.77	63.43, 126.62
PBK	Pevek	70.03° N, 170.92° E	64.09, –135.27	64.14, –135.12	64.22, –134.94
DIK	Dikson	73.25° N, 80.68° E	64.34, 162.7	64.4, 162.72	64.5, 162.67
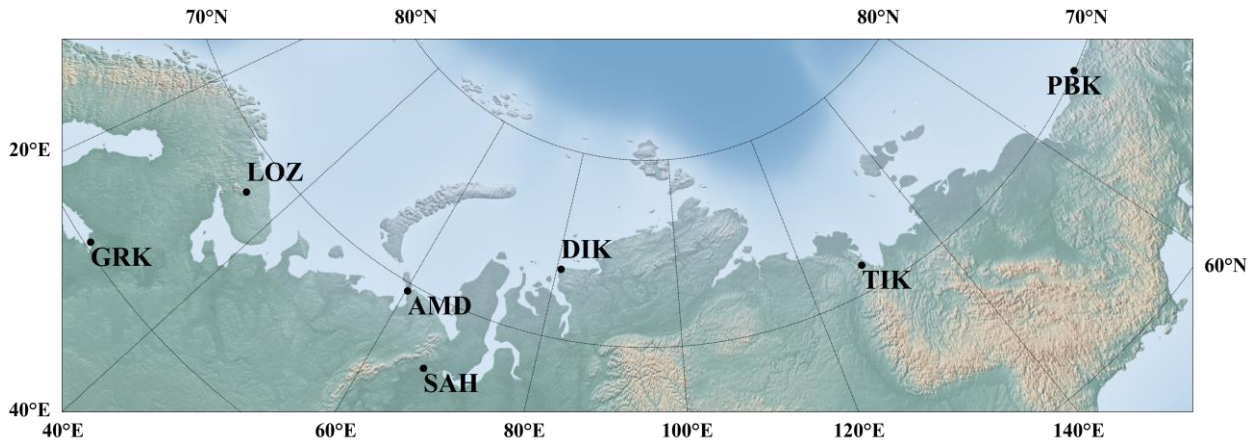
Figure 2. The AARI network of stations for monitoring geophysical conditions in the Arctic, where VSI is carried out
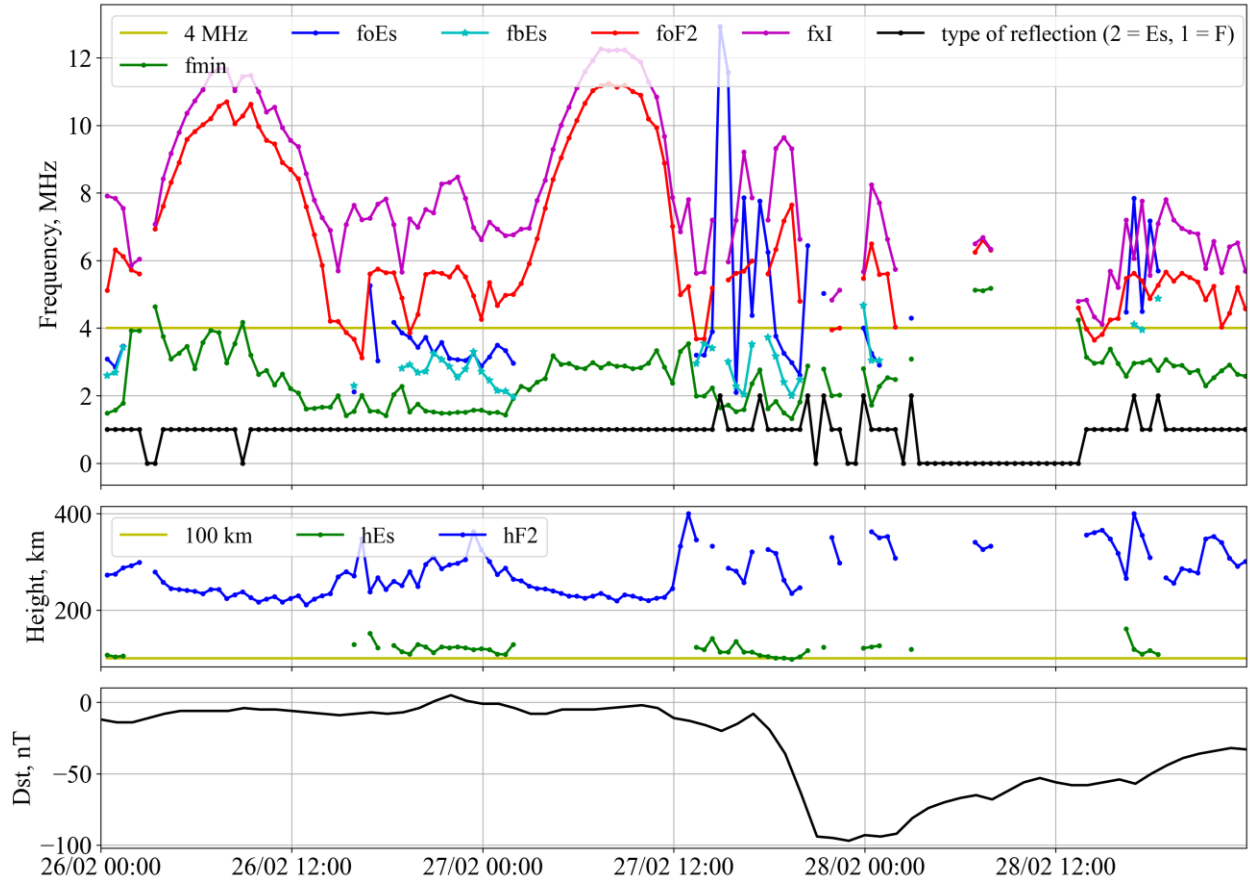
Figure 3. Dynamics of ionospheric parameters according to VSI data from the station Dikson (two top panels) and *Dst* (bottom panel) on February 26–28, 2014. Frequency parameters of the ionosphere: f_{min} — the minimum frequency observed in vertical sounding ionograms; f_oE_s and f_oF2 — the critical frequencies of the ordinary wave of the E_s and F2 layers; f_bE_s — the shielding frequency of the E_s layer; fxI — the highest frequency at which there are reflections from the F-region. The height parameters of the ionosphere: hE_s and $hF2$ are the minimum actual heights of the E_s and F2 layers. The line "reflection type" indicates the condition code of the ionosphere in the F-region up to 4 MHz: no reflection (0), reflection present (1), shielding by the E_{sr} layer (2)

3. RESULTS

Figures 5–8 uniformly present the results of the elliptical model of SCR cutoff used for predicting PCA at VSI stations (see Table 5) during SCR events (see Table 4). The top panel illustrate SCR fluxes of >1.91 MeV protons and >103 keV electrons. Shaded areas suggest that threshold values are higher for these fluxes. Geomagnetic activity is characterized by the indices K_p and *Dst*. Six bottom panels compare the elliptical model with PCA observations at six VSI stations. The model PCA is defined as follows: fluxes of >1.91 MeV protons

The PCA effects are seen to occur mainly during magnetic storms, which feature a negative *Dst* variation and an increase in *PC*. The PCA effects are extended to the lowest latitudes (GRK station) during the storm main and maximum phases when *PC* increases most strongly. The PCA effects can, however, also be observed under weakly disturbed geomagnetic conditions, especially at high-latitude stations. It is significant that during the daytime PCA effects are observed less frequently than at night. This may be due to the day–night asymmetry of SCR penetration.

or >103 keV electrons exceed the threshold values F_{th} of 100 and 2900 $(cm^2 \ s \ sr)^{-1}$ respectively; at the same time, the model geomagnetic cutoff latitude of these protons or electrons is below the geomagnetic latitude of the corresponding station.

Note that the cutoff threshold for 1.91 MeV SCR protons differs from the 2.5 MeV model one, yet this difference is insignificant and can be ignored in a first approximation. Moreover, model cutoff latitudes were calculated for 300 keV electrons, whereas the intensity threshold for electrons was estimated at >100 keV. In this case, it should be noted that the elliptical cutoff model was not designed for 100 keV electrons, so we use a rough approximation of the equality between cutoff boundaries for 100 and 300 keV electrons. We address this problem in the next section, using statistical analysis results.

3.1. SCR interval of February 26 – March 3, 2014.

SCR proton fluxes began to grow rapidly on February 26 and remained above the threshold up until March 2, 2014 (see Figure 5). Electron fluxes exceeded the threshold for a short interval in the first half of February 27. On the same day, a magnetic storm began,
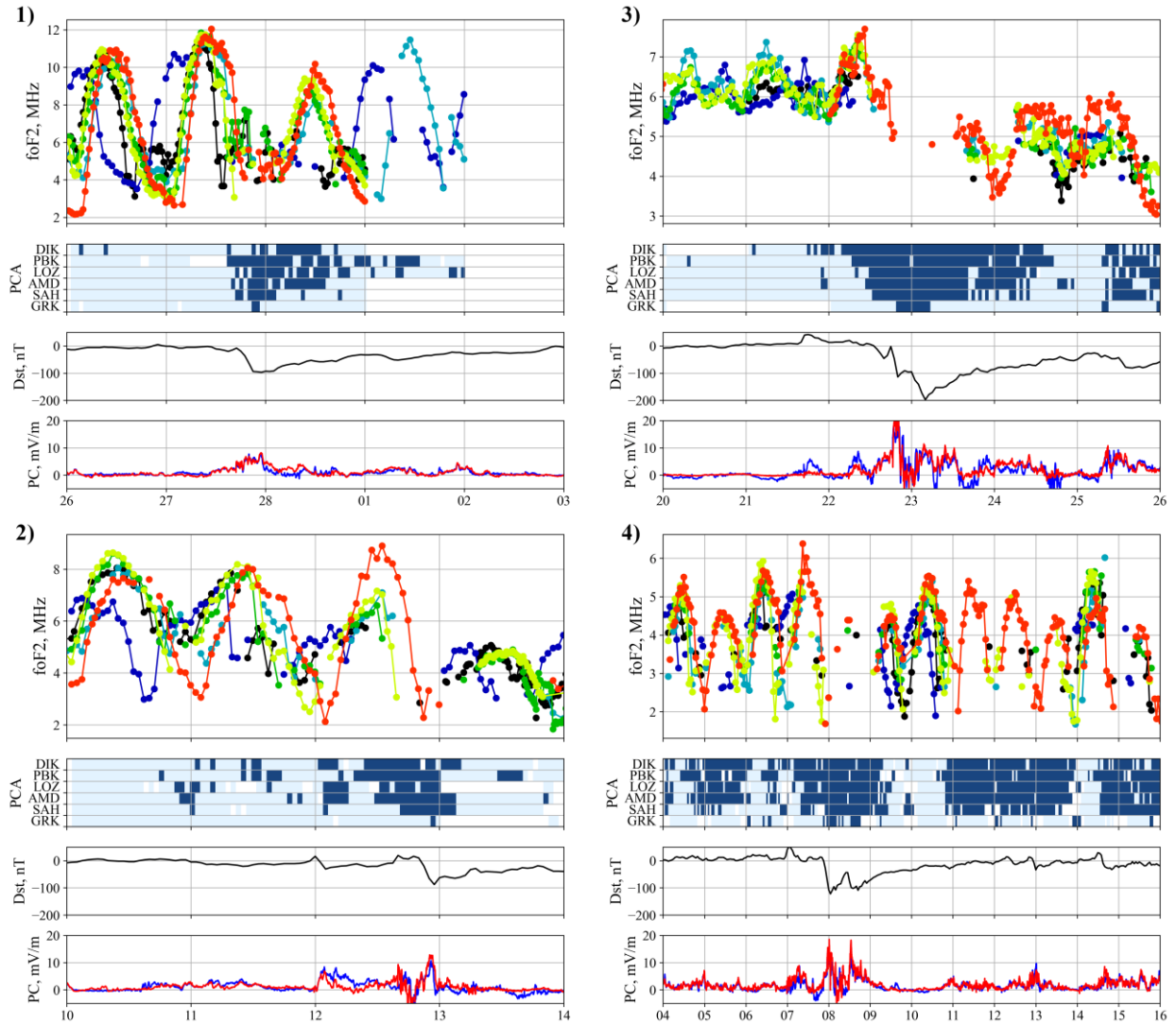
Figure 4. Condition of the ionospheric F-region and geomagnetic indices for the events in February (*a*) and September 2014 (*b*); June 2015 (*c*); September 2017 (*d*). For each event: F2-layer critical frequencies for six VSI stations: DIK (black), PBK (dark blue), LOZ (blue), AMD (green), SAH (yellow), GRK (red). In middle panels is the PCA code for six VSI stations: white — no data, blue — there is a reflection from the F-region, dark blue — no reflection. Bottom panels —*Dst* and *PC* (red — *PCS*, dark blue — *PCN*)

which reached maximum *Dst*=–97 nT on the night of February 27–28 and lasted up until March 2. Thus, most SCR enhancements were accompanied by geomagnetic disturbances.

The elliptical model is seen to quite successfully predict PCA at the high-latitude stations DIK, PBK, LOZ, and AMD. It significant that on March 1 and 2 there is no data on PCA from DIK and AMD, that is why the data was not included in the calculation of statistics determining the accuracy of the model. PCA might have been observed at the high-latitude station DIK since it was recorded at PBK that is close to it in latitude and MLT. This would have improved the statistics on PCA predicted by the model at high latitudes.

For the mid-latitude stations SAH and GRK, the model cannot predict the PCA effect, although the proton cutoff latitudes are quite close, by 1°–3°, to the latitudes of these stations during PCA observation. In general, the accuracy of the model is quite high: *PCP*=0.80 with few false predictions (*FAR*=0.39). The low value of *POD*=0.57 is due to the low accuracy of the model at midlatitudes.

3.2. SCR interval of September 10–14, 2014

Figure 6 presents the parameters and results of the model for September 10–14, 2014. The SCR proton flux in this event exceeded the threshold in the first half of the interval until September 12. The electron fluxes were significantly lower than the threshold ones. A magnetic storm with maximum *Dst*=–88 nT on the night of September 12–13 occurred after an SCR enhancement in the second half of the interval. Thus, in this event the SCR enhancement was observed separately from the magnetic storm.

The accuracy of the model is seen to be low in this case, *PCP* = 0.76. The model predicts many false hour

intervals for the high-latitude station DIK, thereby causing high *FAR*=0.72. On the other hand, the model cannot predict PCA for the mid-latitude stations AMD, SAH, and GRK. Moreover, the model does not predict PCA at all during the September 12–13 magnetic storm because of low proton and electron fluxes relative to the threshold. As a result, its *POD*=0.06 (very low).

3.3. SCR interval of June 20–26, 2015.

Results of the model for this interval are presented in Figure 7. The SCR proton flux in this event exceeded the threshold for almost the entire interval. Electron fluxes remained lower than their thresholds. A powerful magnetic storm with *Dst*=–198 nT at its maximum began on the night of June 21–22, 2015 and lasted up until the end of the interval. Thus, during this event the SCR enhancement was accompanied by both quiet geomagnetic conditions and the magnetic storm.

For this event, the model demonstrates the highest accuracy with *PCP*=0.82. Most hours with PCA were successfully predicted by the model, which yielded *POD*=0.51. At the same time, the number of false predictions is very low, *FAR*=0.19. False predictions of PCA are generally made under undisturbed and slightly disturbed geomagnetic conditions. At the mid-latitude stations SAH and GRK, the model cannot predict most PCA due to two factors. The main one is the intensity of protons whose fluxes are slightly below the threshold. The second factor is an overestimation of the proton cutoff rigidity by 1°–2°.

3.4. SCR interval of September 4–16, 2017.

SCR fluxes, geomagnetic conditions, and model predictions for this interval are shown in Figure 8. Strong enhancements of SCR protons occurred from September 4 to September 13, 2017. A moderate magnetic storm began on September 7 and peaked on September 8 with *Dst*=–122 nT. At that time, the SCR fluxes decreased sharply below the threshold. During the second SCR enhancement, which started during the recovery phase of the September 9 storm, there were intense proton and electron fluxes. During the entire interval, multiple PCA effects were detected, especially at high-latitude stations, both under quiet conditions and during the storm.

For this event, the elliptical model demonstrates a very low accuracy *PCP*=0.41. This is primarily due to the fact that the model cannot predict most observed PCA. For SAH and GRK, the model does not show PCA at all despite intense SCR fluxes. This is presumably because the model overestimates the SCR cutoff latitude for these conditions. Due to the small number of predicted PCA, the probability of false predictions of the model is also very low (*FAR*=0.12).

4. DISCUSSION

Statistical parameters of the elliptical model of predicting PCA for four SCR events are summarized in Table 6. The highest accuracy of the model was obtained for the February–March 2014 and June 2015

events, which occurred with moderate and strong magnetic storms respectively. In both events, model PCAs are associated with enhancements of >1.91 MeV proton fluxes.

For the first event, the model could not predict PCA at mid-latitude stations, although the model SCR cutoff latitudes were quite close to the geomagnetic latitude of the station (see Figure 5). In the second case, the model predicts only a small part of mid-latitude PCAs due to overestimated cutoff latitudes, as well as proton fluxes below the threshold.

Thus, we can conclude that for these events the model overestimates the cutoff latitude for protons by several degrees. This may partly be due to the assumed energy value of >1.91 MeV as opposed to >2.5 MeV. Yet, the small difference between the energies cannot give such a strong difference between cutoff latitudes. Accordingly, for these events, especially for the second one, which occurred in the summer, it is necessary to further specify the model cutoff latitudes, as well as to consider higher-energy SCR protons as a source of observed PCAs.

Low *POD* values are associated with a large number of PCAs on the dayside, which cannot be predicted by the model. They may be caused by intense precipitation of energetic electrons from the radiation belt during magnetic storms. To verify this effect, it is necessary to analyze data from low-orbit satellites, which is the subject of further work.

The model demonstrates relatively low accuracy for moderate magnetic storms during the SCR events in September 2014 and 2017. In the first event (see Figure 6), most PCAs occurred during the moderate magnetic storm when the SCR proton fluxes were slightly lower than the threshold ones, whereas the model cutoff latitudes were lower than the geomagnetic latitude of the VSI stations. In the case of a decrease in the threshold for F_{th} protons to several tens (cm^2 s sr)$^{-1}$, most observed PCAs could be successfully predicted by the model, during both nighttime and daytime MLT, without false predictions for other intervals, i.e. without increasing *FAR*. A small correction of the cutoff latitude at midlatitudes could also significantly increase the number of predicted PCAs, i.e. *POD*.

For the second event, the accuracy of the model is the lowest because it cannot predict most observed PCAs (see Figure 8). This event is characterized by a large number of PCA observations at all latitudes during daytime hours under quiet and slightly disturbed geomagnetic conditions. In this case, SCR proton and electron fluxes were very intense. This suggests that higher energy SCRs whose cutoff latitude is much lower than that for particle energies, employed in the model, contribute to ionization of the upper atmosphere.

Furthermore, the second half of the September 11–16 interval saw weak magnetic storms with small minimum negative *Dst* of several tens of nT. It was, however, at this time that the greatest number of hours with PCA was recorded. On the other hand, the *PC* index at that time increased significantly to 10 mV/m, which indicates a strong disturbance in the polar cap. This event
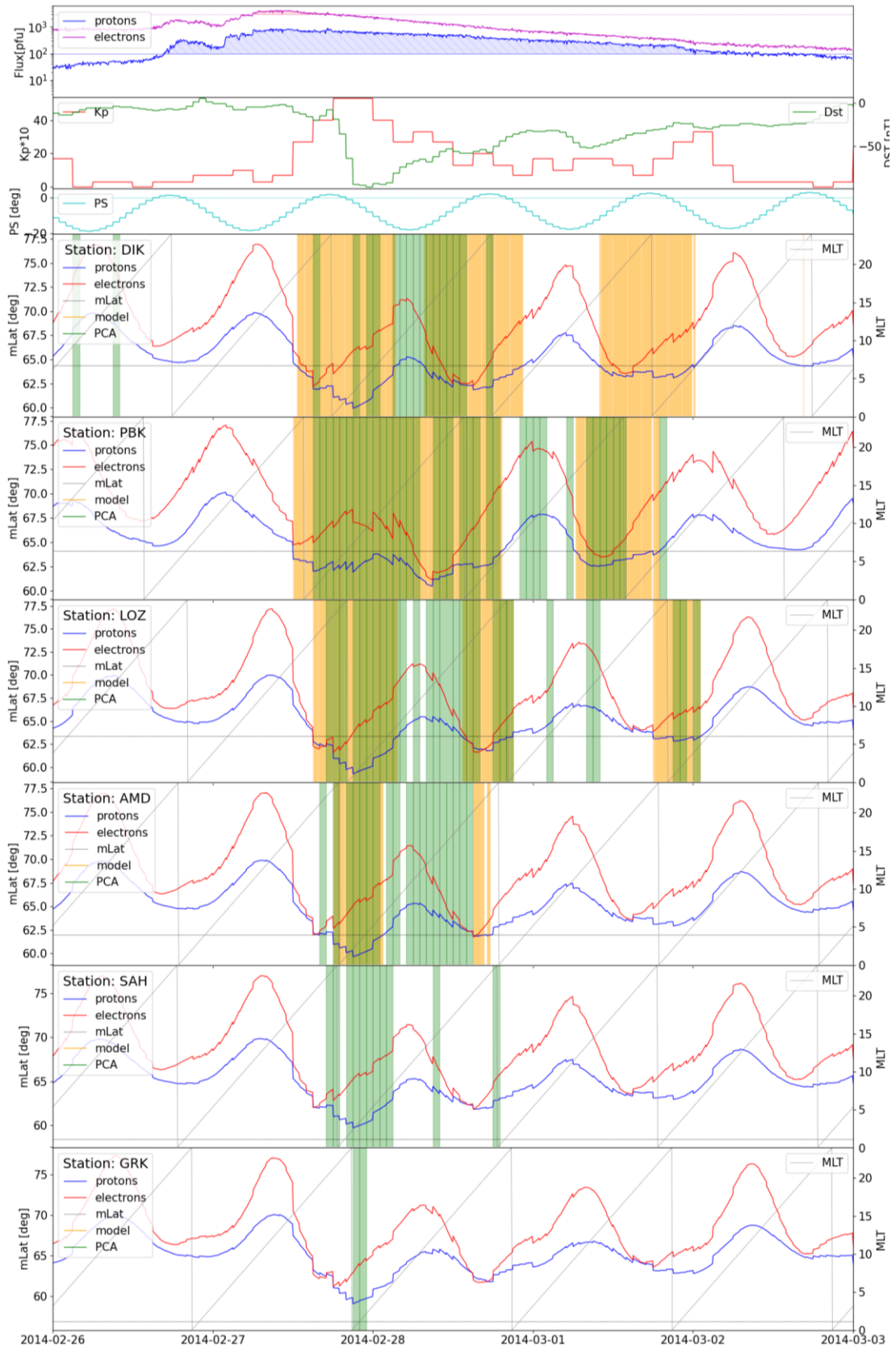
Figure 5. Comparison of the elliptical model with the PCA observations at VSI stations in February–March 2014. From top to bottom: SCR fluxes of >1.91 MeV protons (blue curve) and >103 keV electrons (red curve); (shaded areas — threshold exceeding); geomagnetic indices K_p (red curve) and *Dst* (green curve); dipole tilt angle *PS*; geomagnetic cutoff latitudes of >1.91 MeV protons (blue curve) and >103 keV electrons (red curve) for the MLT station DIK (gray broken line); *mLat* stations (dashed line); the same for AMD; PBK; LOZ; SAH; and GRK. Vertical green rectangles represent the time of PCA observations at the corresponding stations; yellow rectangles mark the model calculation of PCA
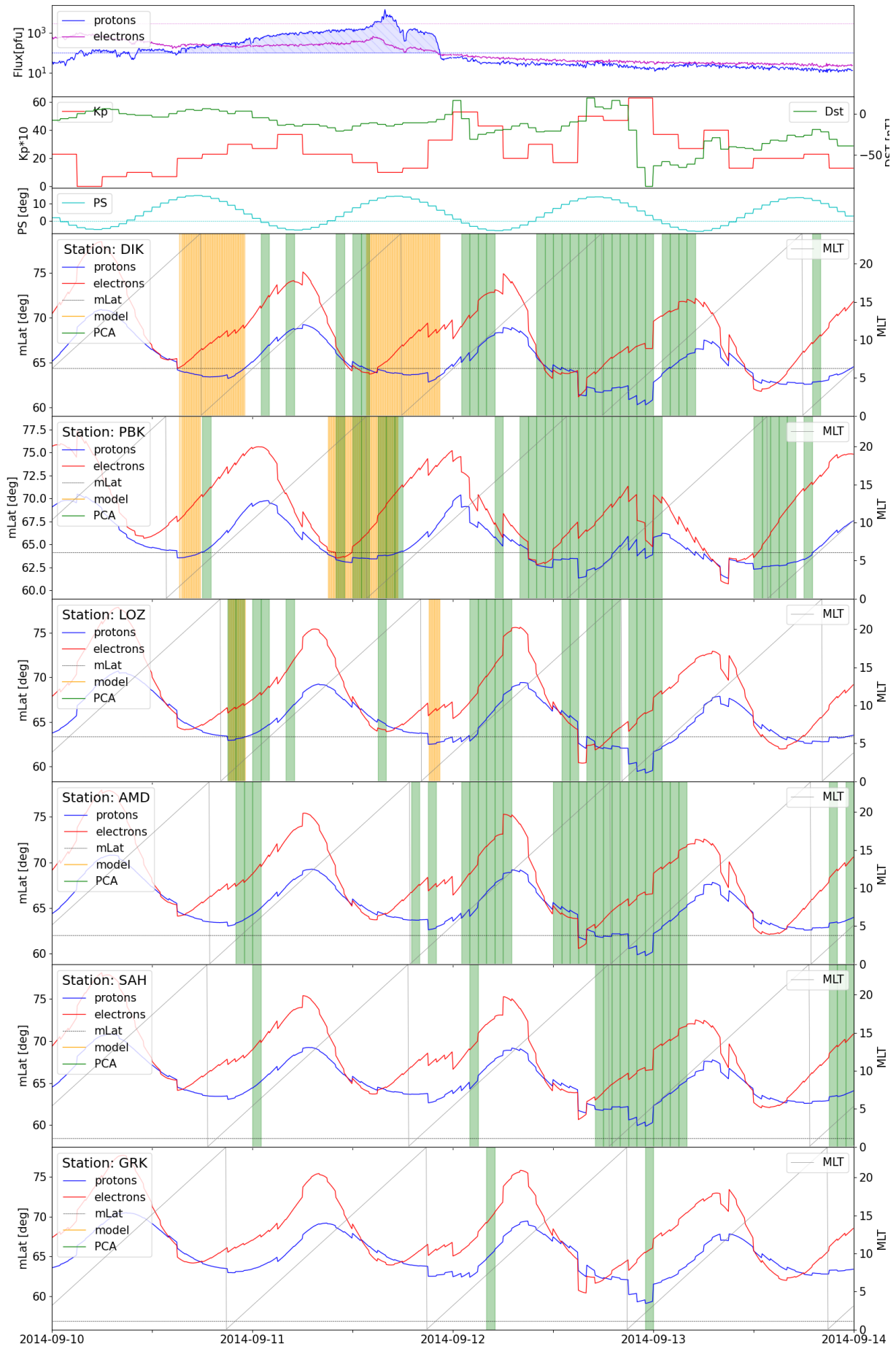
Figure 6. The same as in Figure 5 for September 10–14, 2014
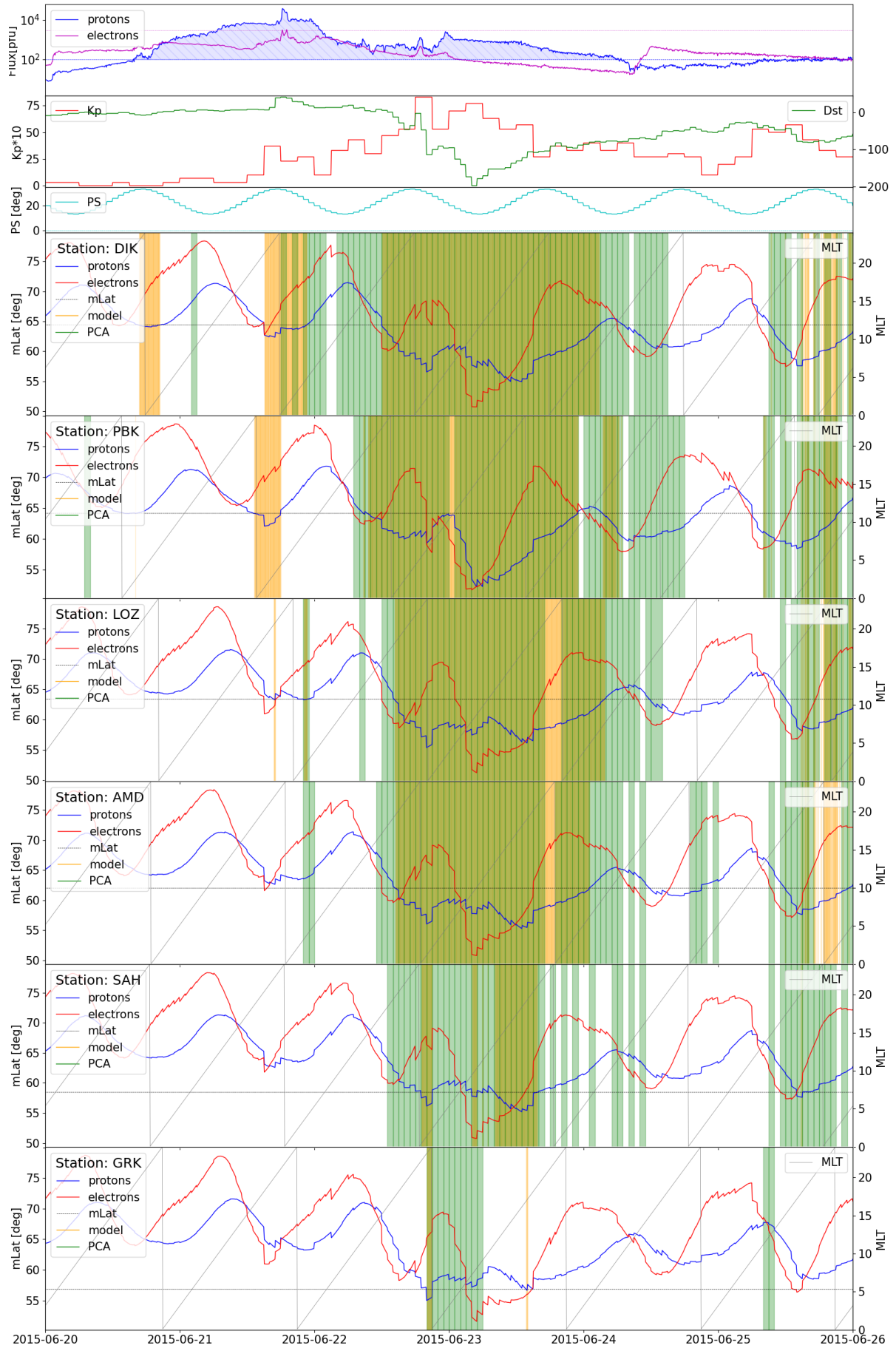
Figure 7. The same as in Figure 5 for June 20–26, 2015
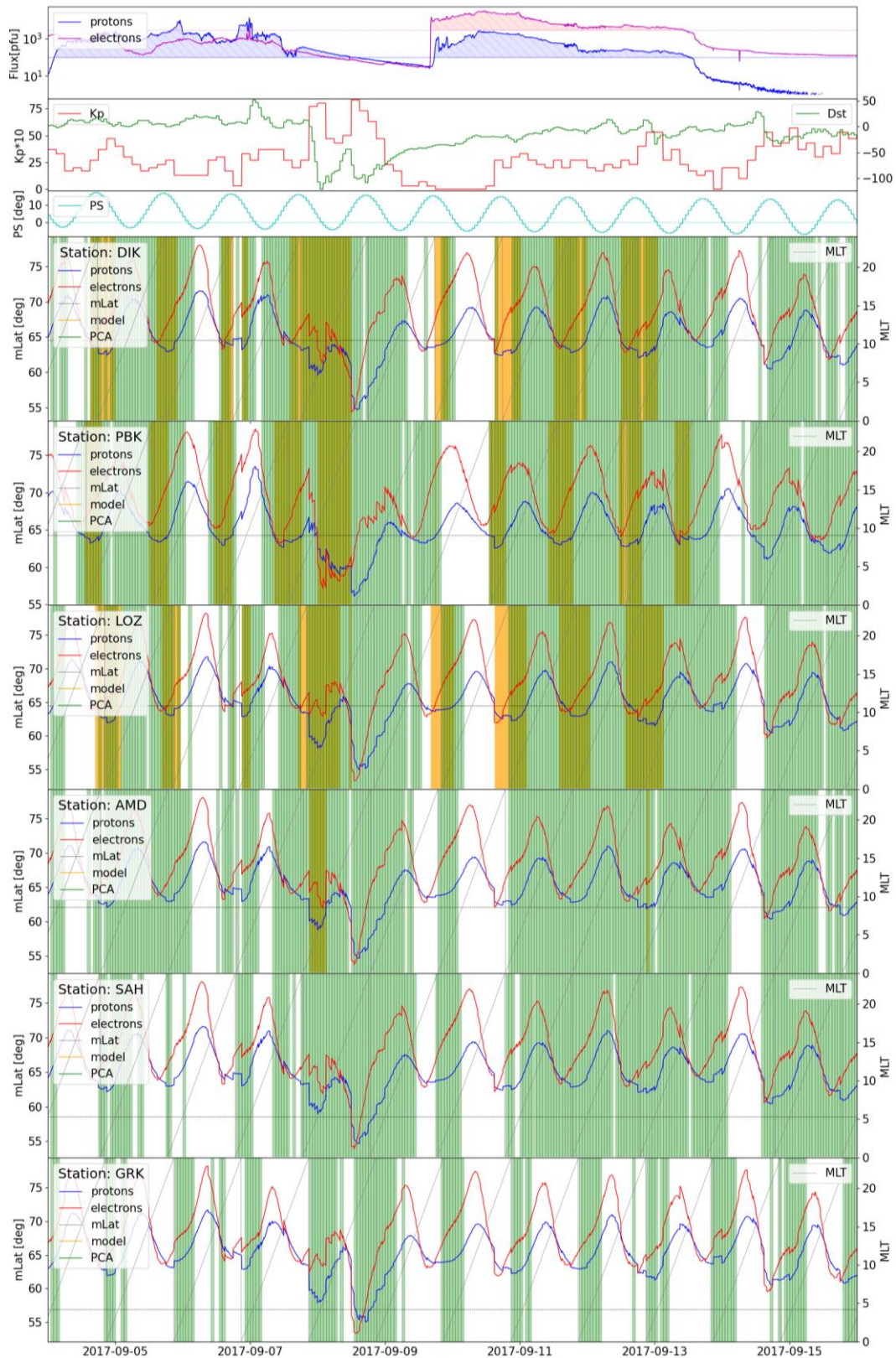
Figure 8. The same as in Figure 5 for September 04–16, 2017

Table 6

Statistical characteristics of the elliptical model accuracy

SCR intervals	PCP	POD	FAR	SCR	Dst_{min}, nT
26.02–03.03.2014	0.8	0.57	0.39	p+e	−97
10.09–14.09.2014	0.76	0.06	0.72	p	−88
20.06–26.06.2015	0.82	0.51	0.19	P	−198
04.09–16.09.2017	0.41	0.17	0.12	p+e	−122

requires a comprehensive analysis of SCR penetration and magnetospheric precipitation with the aid of low-orbit satellites. Moreover, parameterization of the SCR cutoff latitudes in the elliptical model for this interval is likely to require utilizing the *PC* index as an input geomagnetic parameter.

Table 6 shows that SCR electrons are involved in generating PCA in only two events: February–March 2014 and September 2017. That said, in both events the effect of electrons occurred against the background of intense proton fluxes. During the June 2015 event, penetrating SCR electrons of >300 keV could significantly enlarge the statistics on predicted PCA at midlatitudes. Yet, the electron fluxes at that time were much less intense than the threshold ones. In the September 2017 event, almost all predicted PCAs are attributed to intense SCR proton fluxes. That is why the approximation of the equality between the cutoff boundaries for 100 and 300 keV electrons has almost no effect on the prediction result of the elliptical model. On the other hand, the effect of energetic electrons may be significant when adjusting cutoff latitudes and threshold fluxes of SCR protons, using data from low-orbit satellites. This issue is the subject of the next study.

In conclusion, we should note that the elliptical model was developed for a limited range of SCR enhancements in December 2006, for which the geodipole tilt angle *PS* was bounded by the range $-30° \div -10°$. Obviously, extrapolation of the *PS* dependence to the area up to $+30°$ is fraught with inevitable serious errors. With a sharp tilt of the geodipole toward the Sun in summer, the SCR cutoff latitude on the dayside should be significantly lower than in winter when the geodipole is shifted to the nightside. It is, therefore, absolutely necessary to improve the elliptical model in view of new events and data on SCR penetration into the polar cap, obtained in different seasons from low-orbit polar satellites such as POES and Meteor.

CONCLUSION

The elliptical model of SCR cutoff employed to predict the PCA effect, using data from six observation stations located in the Russian Arctic sector, has yielded the following results.

SCRs produce additional ionization of the upper atmosphere at high and middle latitudes. Intense fluxes of >1.91 MeV protons and >100 keV electrons cause electromagnetic waves to scatter in the range to 13 MHz and a strong E_{sr} layer to form at a height of ~100 km.

The elliptical model of SCR cutoff makes it possible to calculate PCA intervals with a high accuracy, *PCP*~0.8. For some events, however, the model accuracy is very low due to the underestimated threshold of SCR proton fluxes and the overestimated cutoff latitude for them. This is associated with the range of geodipole tilt angles in December 2006, when the north polar cap was shifted to midnight.

To improve the elliptical model based on data from the network of VSI stations in the Russian Arctic sector, it is planned to do the following:

- examine other seasons of SCR penetration in which the geodipole tilt angle *PS* reaches 30°;
- consider higher SCR energies as a source of PCA;
- specify intensity thresholds of more energetic SCR particles;
- utilize the *PC* index as an indicator of the geomagnetic disturbance level during magnetic storms.

REFERENCES

Birch M.J., Hargreaves J.K., Senior A., Bromage B.J.I. Variations in cutoff latitude during selected solar energetic proton events. *J. Geophys. Res.: Space Phys.* 2005, vol. 110, A07221. DOI: 10.1029/2004JA010833.

Clilverd M.A., Rodger C.J., Moffat-Griffin T., Verronen P.T. Improved dynamic geomagnetic rigidity cutoff modeling: Testing predictive accuracy. *J. Geophys. Res.* 2007, vol. 112, p. A08302. DOI: 10.1029/2007JA012410.

Dmitriev A.V., Tsai L.-C., Yeh H.-C., Chang C.-C. COSMIC/FORMOSAT-3 tomography of SEP ionization in the polar cap. *Geophys. Res. Lett.* 2008, vol. 35, p. L22108. DOI: 10.1029/2008GL036146.

Dmitriev A.V., Jayachandran P.T., Tsai L.-C. Elliptical model of cutoff boundaries for the solar energetic particles measured by POES satellites in December 2006. *J. Geophys. Res.* 2010, vol. 115, p. A12244. DOI: 10.1029/2010JA015380.

Gold R.E., Krimigis S.M., Hawkins S.E., Haggerty D.K., et al. Electron, Proton and Alpha Monitor on the Advanced Composition Explorer Spacecraft. *Space Sci. Rev.* 1998, vol. 86, pp. 541–562.

Heino E., Partamies N. Observational validation of cutoff models as boundaries of solar proton event impact area. *J. Geophys. Res.: Space Phys.* 2020, vol. 125, e2020JA027935. DOI: 10.1029/2020JA027935.

Jayachandran P.T., Macdougall J.W., Langley R.B., Langley R.B., Sajan C. Mishini. Canadian High Arctic Ionospheric Network (CHAIN). *Radio Sci.* 2009, vol. 44, p. RS0A03. DOI: 10.1029/2008RS004046.

Kallenrode M.-B. Current views on impulsive and gradual solar energetic particle events. *J. Physics G: Nuclear Phys.* 2003, vol. 29, no. 5, pp. 965–981. DOI: 10.1088/0954-3899/29/5/316.

Kalishin A.S., Blagoveshchenskaya N.F., Troshichev O.A., Frank-Kamenetskii A.V. AARI: High-latitude geophysical research. *RFBR J.* 2020, no. 3-4 (107-108), pp. 60–78. DOI: 10.22204/2410-4639-2020-106-107-3-4-60-78. (In Russian).

Kress B.T., Mertens C.J., Wiltberger M. Solar energetic particle cutoff variations during the 29–31 October 2003 geomagnetic storm. *Space Weather.* 2010, vol. 8, p. 5. DOI: 10.1029/2009SW000488.

Little C.G., Leinbach H. Some measurements of high-latitude ionospheric absorption using extraterrestrial radio waves. *Proc. IRE.* 1958, vol. 46, no. 1, pp. 334–348. DOI: 10.1109/JRPROC.1958.286795.

Little C.G., Leinbach H. The Riometer. A device for the continuous measurement of ionospheric absorption. *Proc. IRE.* 1959, vol. 47, no. 2, pp. 315–320. DOI: 10.1109/JRPROC.1959.287299.

Rodger C.J., Clilverd M.A., Verronen P.T., Ulich T. Dynamic geomagnetic rigidity cutoff variations during a solar proton event. *J. Geophys. Res.* 2006, vol. 111, no. A4, p. A04222. DOI: 10.1029/2005JA011395.

Smart D., Shea M. Fifty years of progress in geomagnetic cutoff rigidity determinations. *Adv. Space Res.* 2009, vol. 44, no. 10, pp. 1107–1123. DOI: 10.1016/j.asr.2009.07.005.

Vystavnoi V.M., Makarova L.N., Shirochkov A.V., Egorova L.V. Research into high-latitude ionosphere by vertical sounding with the modern digital ionosonde CADI. *Heliogeophys. Res.* 2013, no. 4, pp. 1–10. (In Russian).

URL: https://cdaweb.gsfc.nasa.gov/ (accessed July 23, 2024).

URL: https://wdc.kugi.kyoto-u.ac.jp/wdc/Sec3.html (accessed July 23, 2024).

This paper is based on material presented at the 19th Annual Conference on Plasma Physics in the Solar System, February 5–9, 2024, IKI RAS, Moscow.